a)

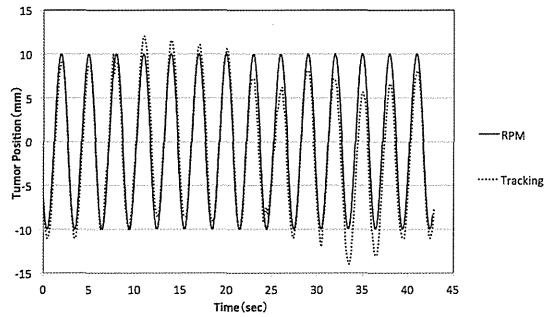

b)

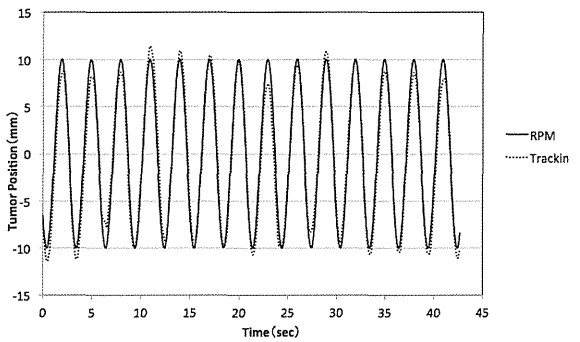

Fig. 3 a) 1 つの ROI のトラッキングで求めた腫瘍位置と b)5 つの ROI のトラッキングを平均して求めた腫瘍位置。

Fig. 4 に 5 つの ROI の配置を示す。

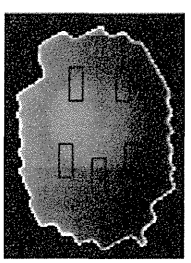

Fig. 4 ROI を 5 つ配置した図。

iii）呼吸波形の違い

呼吸波形を変えてトラッキングを行った結果を Table.1 に示す。どの波形も RPM 波形と比較した場合、2mm 以内の精度であった。

Table.1

波形　周期振幅	差の平均±標準偏差(mm)
①4sec10mm	1.97±1.54
②3sec10mm	1.09±0.70
③4sec5mm	1.03±0.61
④4sec2mm	0.53±0.33

iv）臨床への応用

実際の患者データを用いた結果を次に示す。Fig.5 は ROI の配置と固定照射で腫瘍トラッキングを行った患者①と患者②の結果を示す。患者①のような小さな動きでも、患者②でも両者ともトラッキングできていた。計測により算出した呼吸波形と比べた結果、患者①ではトラッキングと計測による呼吸波形との差は 1.37±0.74 mm、患者②では 0.93±1.58 mm であった。

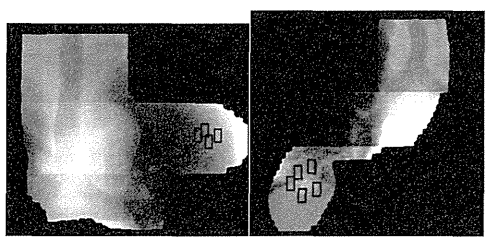

(a①)　　(a②)

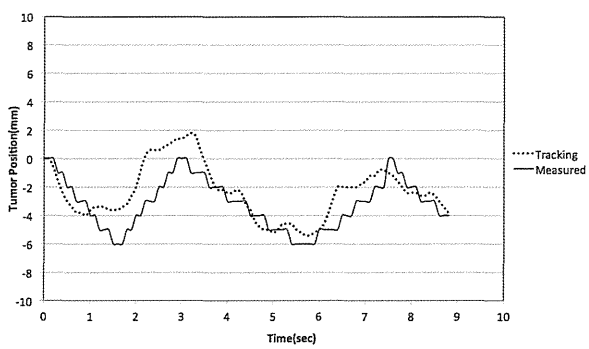

(b①)

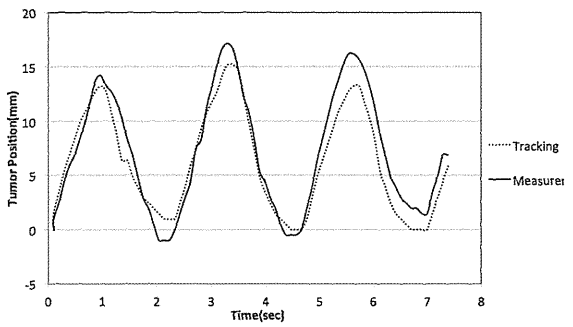

(b②)

Fig.5 （a）患者画像上の ROI の配置例
（b）トラッキング結果
患者①は呼吸性移動な少なく、患者②は呼吸性移動が大きい。Tracking と Measurement は EPID 画像の動き表している。

臨床では、腹壁の動く距離（RPM 波形）と EPID 画像上の腫瘍の動きはファントムのように一定ではないため、患者固有または毎照射時固有の関係式を割り出し、in-house ソフトに組み込んだ。それにより、VMAT 照射時に生じる MLC などによって腫瘍を追えなかった場合に RPM 波形に切り替えることができる。

患者②の固定照射で得られた EPID 画像の上に、ファントムに対する VMAT 照射の動く MLC を重ね合わせた画像（患者 VMAT 画像）結果を Fig.6 に示す。

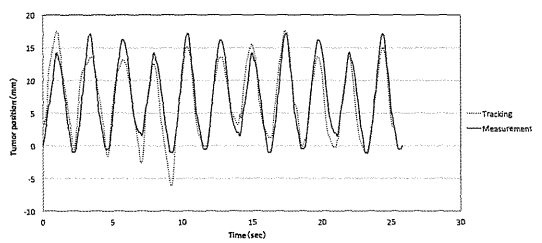

Fig.6 患者②における VMAT プランにした場合の腫瘍トラッキング。

患者 VMAT 画像におけるトラッキングと計測により求めた呼吸波形を比較した結果、差は 0.13±5.36mm であった。

D．考察

本方法で行った正規化相互相関を用いた腫瘍位置の検出法は、EPID 画像内の腫瘍コントラストに大きく影響を受ける。ROI サイズは最小で 5 pixel×10 pixel の大きさが必要であり、VMAT 照射では 10 pixel×20 pixel で解析した。また、腫瘍辺縁の 1 箇所に ROI を設置するより、辺縁複数設置した方がより情報量が多く、より実際の腫瘍位置に近いトラッキングができた。今回は 5 つの ROI を設定し、変動量を平均化することによって、トラッキングの精度も向上できた。また VMAT 照射に本手法を利用するためには、寝台 Rail や椎体との重なりによるコントラストの低下や MLC によって腫瘍が隠れてしまった場合を考え、相関係値が設定の閾値を下回る場合、ROI 内に MLC が入る場合、指定したガントリ角度の場合に RPM 波形に自動的に切り替わるようにソフトを改良した。

臨床画像においては、呼吸の動きの大きさに関わらずトラッキングは可能であり、VMAT プランにも対応できたが、ファントム実験より標準偏差が大きかった。患者 RPM 波形と実際の腫瘍位置にばらつきがあるため、それが影響していると考えられる。

E．結論

VMAT照射中に取得されるEPID画像から腫瘍位置を求めることができた。この方法は治療ビームを用いて画像を取得するために、原理的に画像取得のための被曝線量が生じないという利点がある。

この方法は、固定照射では高い精度を示し、回転照射やVMAT照射においても腫瘍位置を求めることができた。しかし、回転照射では寝台Railや椎体が腫瘍と重なる場合や、VMAT照射では可動するMLCと重なる場合はうまく追うことができなかった。本研究ではこれらに対しては、画像処理によるアーチファクトの軽減や、複数設定したROIの距離平均値を利用することで腫瘍位置精度も向上した。MLCによって腫瘍が完全に隠れてしまう場合は、正規化相互相関の相関値の閾値を設定し、その値を下回る場合にはRPMの移動量を使用するように設定した。また、寝台Railや椎体などに重なるガントリ角度をあらかじめ設定することで、RPMの位置情報をROIに置き換えることを可能とした。これらRPM波形に置き換える作業をソフトのプログラム上に組み込むことによって、VMAT照射において自動的に腫瘍位置情報を取得することができた。また、実患者のEPID画像を用いても本方法で腫瘍位置を検出することができた。

今後臨床データ数を増やすことで、腫瘍の動きと呼吸波形の関連づけや患者固有の動きなども知ることができる。またRPM波形と腫瘍の動きの関係を求めることで、必ずしも直線的な動きをしていないことが実証され、実際の腫瘍の動きを評価することの重要性が示唆された。

F．研究発表

1. 論文発表

なし

2. 学会発表

五月女達子，橋本成世，北村望，木田智士，伊藤康，中島大，大友結子，上原隆三，小塚拓洋，小口正彦．“胸部病変に対するEPID画像を用いた腫瘍位置情報の確認，”医学物理 33 Sup.1, 96, (2013). 第105回日本医学物理学会学術大会，横浜市，平成25年4月11-14日.

Y.Ito, M.Hashimoto, S.Saotome, M.Nakajima, Y.Otomo, N.Kitamura, R.Uehara, T.Kozuka, M.Oguchi; Dose reconstruction in considering of respiratory motion of the target using 4D-CT in VMAT, ASTRO 2013

G.知的財産権の出願・登録状況

1.特許取得

なし

2.実用新案登録

なし

3.その他

なし

厚生労働科学研究費補助金（第３次対がん総合戦略研究事業）

分担研究報告書

強度変調回転照射における腫瘍位置の検出に関する研究:

関心領域の自動設定に関する検討

研究分担者　髙橋　良（公益財団法人　がん研究会有明病院　放射線治療部）

研究要旨

呼吸性移動を伴う病変に対して強度変調回転照射（Volumetric Modulated Arc Therapy: VMAT）を施行する場合、呼吸状態によって線量分布が変化する事が予測されるため、照射中の腫瘍位置を把握する事が重要である。本研究の目的は、VMAT 照射中に電子画像照合装置（Electrical Portal Imaging Device: EPID）を用いて取得した画像に対してフィルタ処理を施す事で、腫瘍位置検出に適した複数の関心領域（Region of Interest: ROI）の設定を自動で行えるシステムの構築が可能か検討する事である。EPID 画像へのフィルタ処理により、腫瘍位置検出を困難にする構造物の除去、腫瘍辺縁等の特徴点の抽出による複数 ROI の自動配置を行い、腫瘍位置変動を算出、評価した。寝台、椎体等の障害陰影を除去し、腫瘍辺縁に ROI 配置が可能となり、EPID 画像のみの腫瘍位置検出精度が向上した。

A. 研究目的

強度変調回転照射（Volumetric Modulated Arc Therapy: VMAT）はガントリが回転しながら多分割コリメータ（Multi Leaf Collimator: MLC）の開口形状やガントリ回転速度、線量率を動的に変化させる照射方法である。呼吸性移動を伴う病変に対し VMAT を施行する場合、呼吸状態によって線量分布が変化する事が予測されるため、治療中の腫瘍位置を把握する事が重要である。

分担研究者（五月女達子）による前年度の研究結果より、照射中に電子画像照合装置 aS1000（Electrical Portal Imaging Device: EPID）により得られた画像に対して正規化相互相関（Normalized Cross Correlation: NCC）を用いて腫瘍位置を検出し、一定の成果を得る事が出来た。しかし、回転照射や VMAT では腫瘍位置の検出が困難な場合もあった。このような腫瘍位置の検出が困難な例に対して、複数の関心領域（Region of Interest: ROI）の設定や、腫瘍位置の検出に適した ROI 配置を行う事が出来れば、腫瘍位置の検出精度の向上が期待できる。本研究の目的は、EPID 画像にフィルタ処理を施し、腫瘍位置検出に適した複数の ROI 配置を自動で行えるシステムの構築が実現可能であるか検討する事である。

B. 研究方法

本研究では、胸部動体模擬ファントム

Model 008A（CIRS 社製）を用いて呼吸性移動を伴う胸部病変を模擬した。ファントム内には、直径 3cm の模擬腫瘍を挿入し、呼吸設定を振幅±5mm、周期 4 秒の正弦波形として動作させながら Discovery ST Elite（GE 横河メディカルシステムズ社製）で 4 次元 CT 画像を取得した。CT 撮影時には、呼吸同期制御装置（Real Position Management: RPM）の呼吸波形も同時に取得した。得られた 4 次元 CT 画像に対し、固定前方照射・回転照射・VMAT の治療計画を Eclipse version 10（Varian Medical Systems 社製）で立案し、直線加速装置 Clinac21EX（Varian Medical Systems 社製）で照射した。各照射条件は、X 線エネルギーを 6MV とし、固定前方照射では線量率 300MU/min、回転照射では線量率 300MU/min、ガントリ回転を 320 度から 179 度の時計回りの 1 アーク、コリメータ角度は 30 度とした。VMAT は、計画時設定線量率の上限値を 600MU/min にて計画されたもので、ガントリ回転、コリメータ角度は回転照射時と同様のものとした。照射中には腫瘍位置の検出に必要となる EPID 画像を連続的に取得した。EPID の線源検出器間距離（Source Detector Distance: SDD）は 160cm、画像収集のフレームレートは 10fps（frame per second）とした。

本研究では、(1) EPID 画像のフィルタ処理、(2) NCC に用いる複数 ROI の自動選択法による腫瘍位置検出の検討を行った。

(1) EPID 画像のフィルタ処理

分担研究者（五月女達子）の前年度の研究結果から、照射中に取得される EPID 画像には様々な構造物（寝台、椎体等の障害陰影）が写り込むため腫瘍位置検出を困難にする場合が存在する。特に、回転照射時にはガントリ回転に伴い障害陰影が写り込む事により、NCC の低下を引き起こし腫瘍位置の検出精度が低下する。障害陰影による影響を減らすために、ガントリ回転に対して垂直方向にエッジ強調をかけたフィルタ処理画像を作成した。EPID 画像から算出される腫瘍位置変動をフィルタ処理の有無で比較した。

(2) NCC に用いる複数 ROI の自動選択法

腫瘍位置の検出に用いる ROI の自動配置を可能にする為、EPID 画像に対してフィルタ処理を施した。フィルタ処理は、分担研究者（五月女達子）の前年度の研究結果から腫瘍辺縁をよく描出し、かつ胸部病変周辺の血管陰影の検出を想定し、エッジ、テクスチャ強調が可能な Variance フィルタを選択した:

$$\mathrm{Var}(I_{p_j}) = \frac{1}{M-1}\sum_{\xi \in I_{p_j}} \left(I_{p_j}(\xi) - \bar{I}_{p_j}\right)^2 \qquad 1)$$

ここで、EPID 画像内でフィルタ処理を行う位置$\{p_j \mid j = 1, 2, \ldots, N\}$とした時、$I_{p_j}$は$p_j$におけるピクセル値であり、ピクセル数 M を含むフィルタサイズ領域を示す。$\bar{I}_{pj}$はI_{pj}内の全ピクセル値の平均値である。本研究におけるフィルタサイズは、NCC を算出する際の ROI サイズと同サイズに設定した。Variance フィルタ処理を施した EPID 画像は、NCC 算出と同サイズの領域内で腫瘍辺縁等のテクスチャが強調されているため、フィルタ処理画像内のピクセル値が高い位置から順に ROI の配置を行った。ROI を複

数個配置する際、ROI 選択時に除外規定を設け、選択される ROI 間距離が一定に保たれるようにする事で ROI がある一部に集中する事を避ける処理を行った。EPID 画像のフレーム毎に ROI を 100 個ずつ配置した。選択された ROI から NCC を用いた腫瘍位置変動を算出した。腫瘍位置変動の算出には、NCC が 0.84 以上の ROI のみを採用した。

EPID 画像から算出した腫瘍位置変動との比較には、EPID 画像取得時の呼吸設定である正弦波を用いた。腫瘍位置変動の評価は、正弦波との差の平均と標準偏差を用いて行った。

C. 研究結果

EPID 画像に対するフィルタ処理画像と ROI の自動配置の例を Fig. 1、Fig. 2 に示す。Fig. 1 より、寝台、椎体等の障害陰影が除去され、腫瘍のみを抽出した画像が得られた。Fig. 2 より、フレーム毎に腫瘍辺縁に均等に ROI が配置されている事が確認できた。

Fig. 3 に各照射条件における呼吸設定である正弦波と EPID 画像から算出した腫瘍位置変動を示す。固定前方照射において、正弦波との差の平均はフィルタ処理の有無でそれぞれ、0.00 ± 0.45mm、0.00 ± 0.48mm、回転照射ではそれぞれ-31.31 ± 20.34mm、-3.63±3.65mm だった。

フレーム毎に算出された腫瘍の移動量と正弦波の移動量との差をそれぞれ Fig. 4、Fig. 5 に示す。固定前方照射の場合、正弦波との移動量の差の平均はフィルタ処理の有無でそれぞれ、-0.01 ± 0.11mm、0.00 ± 0.13mm、回転照射ではそれぞれ-0.06 ± 0.47mm、-0.01±0.21mm だった。

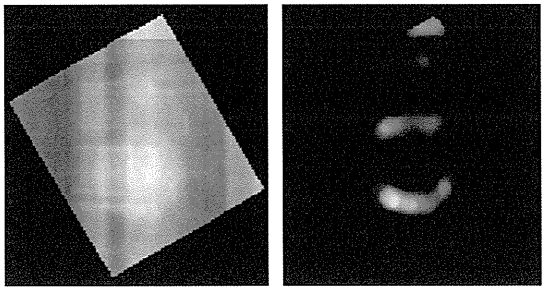

Fig. 1 EPID 画像に対してエッジ強調を施し障害陰影を除去した画像
(a) EPID 画像 (b) エッジ強調画像

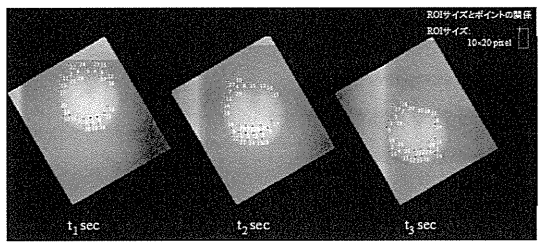

Fig. 2 EPID 画像に対して 30 個の ROI を自動配置した例。EPID 画像のフレーム毎に ROI が腫瘍辺縁を含む位置に配置されている。EPID 画像中のポイントは、ROI の左上隅の座標を示す。

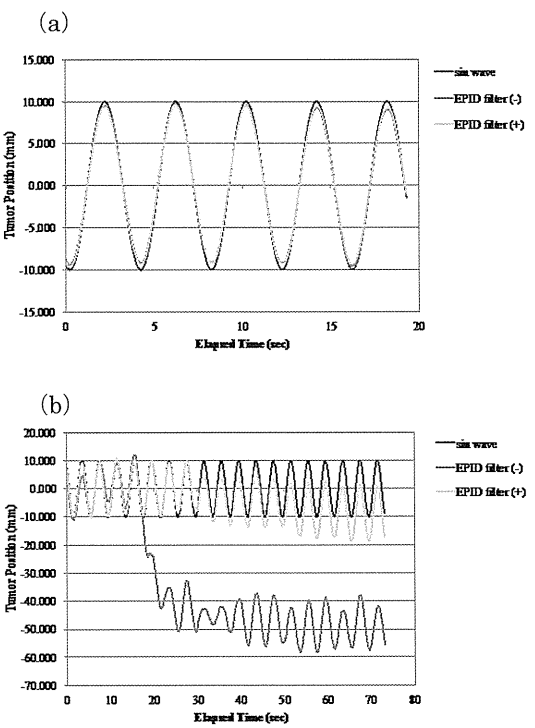

Fig. 3 EPID 画像から算出した腫瘍位置変動
(a) 固定前方照射、(b) 回転照射

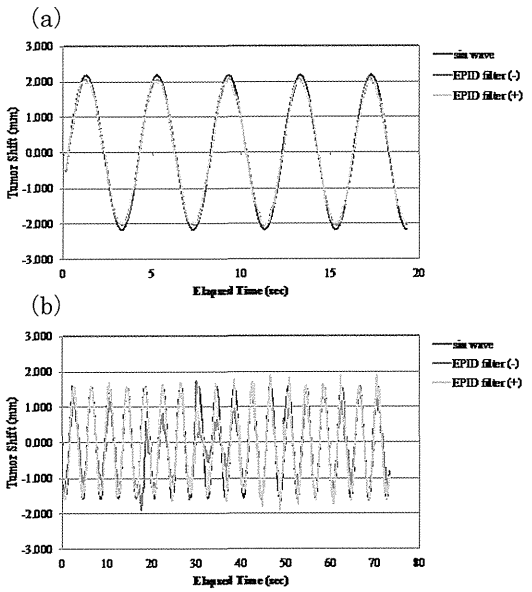

Fig. 4 EPID 画像から算出した腫瘍移動量
(a) 固定前方照射、(b) 回転照射

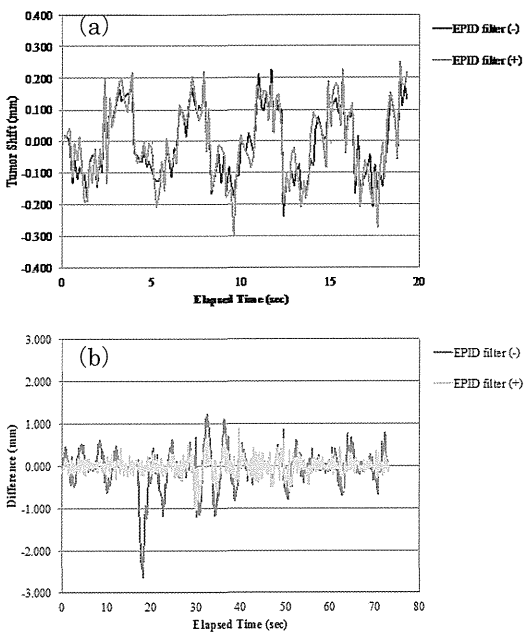

Fig. 5 正弦波移動量と腫瘍移動量との差
(a) 固定前方照射、(b) 回転照射

D. 考察

EPID 画像に対して、エッジ、テクスチャ強調が可能な Variance フィルタ処理を施す事で腫瘍辺縁に対して複数ROIを自動で配置する事に成功した。しかし、Fig. 3、Fig. 4 の回転照射の結果から複数 ROI を用いた場合でも、寝台、椎体等の腫瘍以外の障害陰影の影響により腫瘍位置算出に誤差を生じる結果となった。これは、腫瘍位置検出に用いている現手法である NCC の類似度計算がガントリ回転に対して垂直方向の類似度のみを評価しており、寝台、椎体等のガントリ回転方向に対して平行移動する構造物がROI内に写り込んでしまうため、複数ROIを設定した場合であっても検出精度が低下したと考えられる。この影響に対しては、ガントリ回転に対して垂直方向にエッジ強調させたフィルタ処理画像を用いる事で腫瘍位置検出精度が改善した。フィルタ処理画像を用いた腫瘍位置検出の妥当性については、固定前方照射の結果から、算出される腫瘍位置、移動量共にフィルタ処理を施していない EPID 画像と同等の結果が得られており問題は無いと考えられる。

腫瘍位置変動の算出精度は、フレーム毎の移動量の算出精度に大きく依存する。本研究においても、回転照射時にフィルタ処理を施す事で改善はみられたものの移動量の差が大きい箇所で腫瘍位置変動のベースラインを変位させてしまう結果となった。ベースラインの変位や周期的にみられる差は、フィルタの改良や EPID の解像度を高くする事で改善できると考えられる。

VMAT 照射において、ROI に MLC が入り込む際の処理が作成できなかったため検討できていないが、本手法で ROI 配置を行うと Fig. 6 のように MLC を避けて腫瘍辺縁に ROI を配置する事が確認できている。今後、NCC による類似度計算時に MLC が含まれた際の処理を構築する事で VMAT への応用が可能であると考えられる。

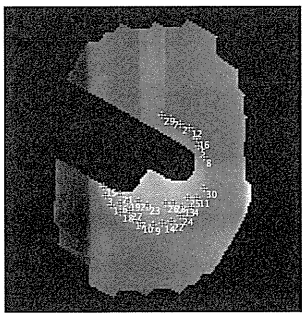

Fig. 6 VMAT 時の ROI の自動配置の様子。
EPID 画像に対して 30 個の ROI を配置した例

本手法における腫瘍位置の検出は、RPM などの腹壁運動と腫瘍の相関性を考える必要がなく、直接的に腫瘍位置の把握が可能なため腹壁運動との相関の無い部位への応用も可能である。今後更なる精度向上への検討を進めていきたいと考える。

E. 結論

EPID 画像に対して腫瘍位置検出に弊害を及ぼす構造物の影響を減らすフィルタ処理を施す事で、腫瘍位置検出精度が向上した。また、腫瘍辺縁等のテクスチャ強調を行う事で、NCC に用いる ROI の自動配置に成功した。EPID 画像にフィルタ処理を施し、腫瘍位置検出に適した複数の ROI 配置を自動で行えるシステムの構築が実現可能である事が示唆された。

F. 研究発表

1. 論文発表

Hidenobu Tachibana and Ryo Takahashi, "Quantitative analysis of geometric information from an end-to-end examination of IMRT and VMAT using the optimal selection method." Med. Phys. 40, 061709 (2013)

G. 知的財産権の出願・登録状況

なし

Ⅲ 研究成果の刊行に関する一覧表

研究成果の刊行に関する一覧表レイアウト

書籍

著者氏名	論文タイトル名	書籍全体の編集者名	書　籍　名	出版社名	出版地	出版年	ページ

雑誌

発表者氏名	論文タイトル名	発表誌名	巻号	ページ	出版年
Tachibana H, Takahashi R	Quantitative analysis of geometric information from an end-to-end examination of IMRT and VMAT using the optimal selection method	Med. Phys.	40(6)	061709	2013

Ⅳ 研究成果の刊行物・別刷

Quantitative analysis of geometric information from an end-to-end examination of IMRT and VMAT using the optimal selection method

Hidenobu Tachibana[a)]
Department of Radiation Oncology, University of Texas Southwestern Medical Center, 5801 Forest Park Road, Dallas, Texas 75390-9183

Ryo Takahashi
Department of Radiation Oncology, Cancer Institute Hospital of the Japanese Foundation of Cancer Research, Tokyo 1358550, Japan

(Received 18 January 2013; revised 2 April 2013; accepted for publication 29 April 2013; published 22 May 2013)

Purpose: Gamma index, distance-to-agreement, and dose difference (DD) are commonly used to evaluate planar dose distributions. In this evaluation, the agreement between calculated and measured dose distributions can be susceptible to steep dose gradients along another axis perpendicular to the evaluation plane. Visual registration of the measured dose distribution may be performed to achieve better agreement, although doing so might lose geometric information related to beam targeting in an end-to-end test of intensity modulated radiation therapy (IMRT) and volumetric modulated arc therapy (VMAT). The optimal selection (OS) method was developed to take into consideration a dose distribution in three-dimensions, and also to quantitatively analyze geometric information along with better agreement.

Methods: The OS method was composed of two steps. These steps were based on two algorithms, the gamma index and DD, to (1) find the best-matched plane, which is parallel to the planar measured dose distribution and is reconstructed by a volumetric dose distribution calculated by a treatment planning system; and (2) to get shifts and rotation along with better agreement between the calculated and measured dose distribution, compared with the planar dose distribution from the test. The OS method computes shifts and rotation against a user-defined coregistered location for the measured dose distribution. Thirteen prostate IMRT plans (two planes per plan for a total of 26 planes) were analyzed retrospectively to compare the pass ratios of DD and gamma index evaluations with and without the OS method. The computed shifts and rotations were evaluated.

Results: Compared with the method without OS, the average pass ratios of DD and gamma index with the OS method increased by 8.2% and 5.7%, respectively, in the dose region from 30% to 100%. A particular result from one of the planes showed an increase of 43.5% and 32.5% in the pass ratios of DD and gamma, respectively, with the OS method in the same dose region. The shifts in the x-, y-, z-axes and rotation, which were computed using the OS method, were 0.5 ± 0.6, 0.3 ± 0.5, 1.0 ± 1.1 mm, and $0.3 \pm 0.3°$, respectively. In terms of the comparatively large difference between the z-shift and the x- and y-shifts, an additional geometric test was performed. A systematic error of 0.7 mm in the z-axis was found at the location of the film placed in the phantom that we used.

Conclusions: The OS method improved the quality of the end-to-end test of IMRT and VMAT plans by providing additional information regarding shifts and rotation, which were calculated and found to be in better agreement. © *2013 American Association of Physicists in Medicine.* [http://dx.doi.org/10.1118/1.4805103]

Key words: IMRT, VMAT, end-to-end examination, optimal selection method, geometric information

I. INTRODUCTION

The plan verification measurement of intensity modulated radiation therapy (IMRT) and volumetric modulated arc therapy (VMAT) is regarded as an end-to-end test to determine the accuracy of dose delivery and beam targeting. In the evaluation analysis of the test, several algorithms, such as gamma index,[1] distance-to-agreement (DTA), and dose difference (DD) are commonly used to assess two-dimensional (2D) dose distributions. Using these algorithms, the error of beam targeting is included as the error of dose delivery throughout the test. In film dosimetry for plan verification, the film should be accurately placed within a measurement phantom and pin pricked or otherwise marked at known locations. Subsequently, absolute positioning for film is generally performed by specifying two pairs of marks on the film, defining two lines, the crossing point of which defines the isocenter on the film.[2] However, manual registration for the film should be done visually to achieve a better result, even though the measurement is an end-to-end test.[3] Namely, visual registration is

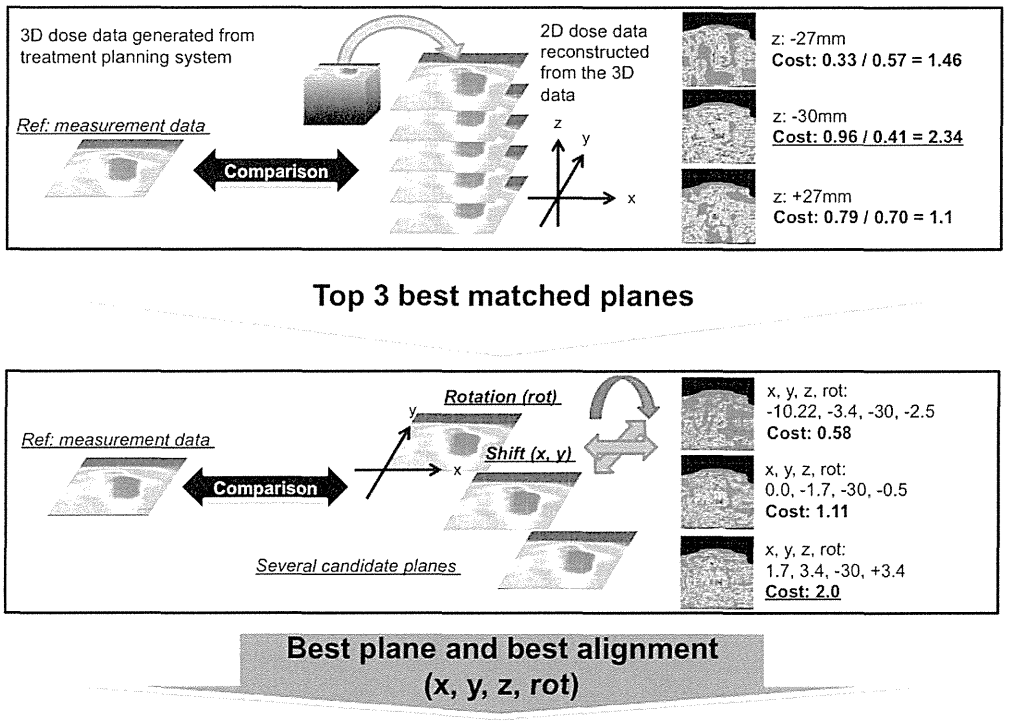

FIG. 1. A schematic representation of the OS method.

nonquantitative and might lose important geometric information in the end-to-end test. Similar care must be taken when using 2D detector arrays.

Dose distributions calculated by a treatment planning system are volumetric data, which are composed of dose values with three-dimensional (3D) coordinates. In the analysis of plans, dose distributions in 2D are often exported and used for comparison against measurements because dosimetry using film[4–9] and 2D detector arrays[10–13] provide a planar dose distribution. Currently, there are some commercially available 3D detector arrays,[14–17] but they are "pseudo" 3D detector arrays because they use mathematical interpolation algorithms with the measurement data from multiple 2D detector arrays to create a volumetric dose distribution. Gel dosimetry[18,19] represents real dose distributions in 3D. Nonetheless, measurement efficiency is poor and thus is practically insufficient for clinical plan verification measurement. The comparison between a calculated and measured dose distribution in 2D could include errors of dose delivery and beam targeting along another axis perpendicular to the evaluation plane. If there is a steep dose gradient region in the axis and errors due to isocenter laser misalignment, phantom setup, and film setup, then the agreement in the region could dramatically decrease, even though the errors were not derived from the evaluation plane.

New gamma index algorithms have been developed that incorporate pass–fail criteria for both DTA and DD analysis of 3D dose distributions.[20–24] However, the error of beam targeting is represented as the error of beam delivery in these algorithms, and these algorithms do not show geometric information of the errors related to beam targeting.

In this study, we designed and developed the optimal selection (OS) method to take into account dose distributions in 3D and to quantitatively analyze geometric information along with better agreement in the end-to-end test.

II. METHODS AND MATERIALS

II.A. The OS method

A schematic representation is shown in Fig. 1.

Before the calculation of the OS method, a volume dose distribution calculated by a treatment planning system and a planar dose distribution from a film or a 2D detector array were loaded, and the measured dose distribution was coregistered using landmarks.

In the first step of the OS method, multiple planes of the calculation parallel to the measurement plane were reconstructed from the volume dose distribution. In the OS method, the axis perpendicular to the measurement plane was defined as the z-axis. The spatial resolution of the volume dose distribution depends on dose calculation grid size in the treatment planning system. Then, the reconstructed calculation planes were compared with the measurement plane using the 2D gamma index algorithm[1] and scored to choose the top three best-matched planes. In the experiments in this paper, 3% for DD and 3 mm for DTA were used as the criteria for evaluation. A score was calculated as

$$\mathrm{Score}_{\mathrm{gamma}} = \frac{(\mathrm{Pass\ ratio})_{\mathrm{gamma}}}{\frac{1}{N_x}\frac{1}{N_y}\sum_{x=1}^{N_x}\sum_{y=1}^{N_y}\mathrm{Value}(x, y)_{\mathrm{gamma}}}, \quad (1)$$

where $(\mathrm{Pass\ ratio})_{\mathrm{gamma}}$ denotes the pass ratio in the evaluation using the gamma index algorithm. $\mathrm{Value}(x, y)_{\mathrm{gamma}}$

denotes the value of the gamma index with the coordinate (x,y) in the evaluation plane. N_x and N_y denote the rows and the columns of the evaluation plane, respectively. The analysis of the 2D gamma index uses a pass–fail criterion of both the dose difference and distance-to-agreement, which depends on their amplitudes, but the index value is independent of direction. Thus, the score is unsusceptible to errors of beam targeting, such as setup errors using film and a phantom and isocenter laser alignment error.

The second step was performed to find the best plane for comparison with x- and y-shifts and rotation. First, x- and y-shifts and rotation candidates were prepared for the three best-matched calculation planes. Second, a calculation plane was reconstructed with each of the candidates using B-spline interpolation. Finally, the reconstructed calculation plane was compared with the measurement plane using the DD algorithm to calculate a score using the following:

$$\mathrm{Score}_{\mathrm{DD}} = \frac{(\text{Pass ratio})_{\mathrm{DD}}}{\frac{1}{N_x}\frac{1}{N_y}\sum_{x=1}^{N_x}\sum_{y=1}^{N_y}\mathrm{Value}(x,y)_{\mathrm{DD}}}, \quad (2)$$

where $(\text{Pass ratio})_{\mathrm{DD}}$ and $\mathrm{Value}(x,y)_{\mathrm{DD}}$ denote the pass ratio of DD and the value of DD with the coordinate (x,y) in the plane, respectively. N_x and N_y denote the rows and the columns of the evaluation plane, respectively. The same processes were repeatedly executed for the calculation planes with the other candidates of the shifts and rotation. In this paper, 3% was set as the criterion of the evaluation. Finally, the OS method gives the xyz-shifts and rotation on the xy-plane against the user-defined coregistered location for the measured dose distribution. The score is affected drastically when the calculation plane is shifted and rotated compared with the measurement plane.

In the OS method, the gamma index algorithm was utilized to determine the top three matched calculation planes parallel to the evaluation plane. Then, the DD algorithm was used to find the best shifts and rotation for the calculation plane. The DD step needs to be processed with many combinations of shifts and rotation, which exceeds the number of combinations for the gamma index step. However, because the DD process is faster than that of the gamma index, the use of the DD evaluation in the second step can be used to make faster computations over the total steps taken.

The OS method was implemented using commercial software, Simple IMRT Analysis Version 2.0 (Triangle Product, Ishikawa, Japan), using the Java programming language. Dose difference, DTA, and gamma index were performed using the software followed by visual evaluation and statistic assessment of pass ratios.

II.B. Preliminary study of the OS method

The purpose of the preliminary study is to check if the OS method works properly in a simple environment before a clinical study. A simple dose distribution in 3D was generated in an Eclipse treatment planning system version 10.0 (Varian Medical Systems, Palo Alto, CA). The dose calculation grid size was set to 2.5 mm. The setup included a treatment field with a symmetric 10×10 cm^2 jaw size, 0° gantry angle that irradiated an I'mRT Phantom (IBA Dosimetry, Schwarzenbruck, Germany) consisting of water equivalent RW3 material (1.045 g/cm^3 density). A dose of 2.0 Gy was prescribed at isocenter, which was located at a depth of 9 cm. As shown in Fig. 2, the plane perpendicular to the central axis of the beam was chosen as the evaluation plane. First, the volume dose distribution was loaded as the reference image. Similarly, the same dose distribution was loaded as the comparative image. Second, the planar dose distribution on the isocenter plane was reconstructed for the reference image. As the comparative image, the planar dose distribution was reconstructed with a combination of the following xyz-shifts and rotation

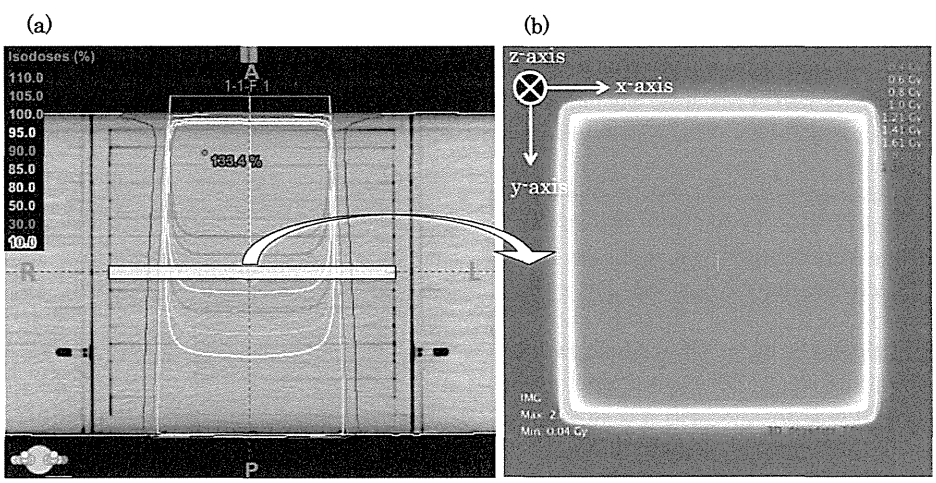

FIG. 2. Dose distribution used in the preliminary study. (a) The dose distribution at the isocenter on the axial plane. The dose distribution in 3D was generated using a treatment field with a symmetric 10×10 cm^2 jaw size, 0° gantry angle that irradiated an I'mRT Phantom (IBA Dosimetry, Schwarzenbruck, Germany) consisting of water equivalent RW3 material (1.045 g/cm^3 density). A dose of 2.0 Gy was prescribed at isocenter, which was located at a depth of 9 cm. (b) The coronal dose distribution on the isocenter plane was reconstructed after the dose distribution in 3D was loaded. The horizontal and vertical axes of the planar dose distribution are x-axis and y-axis, respectively. The axis of depth is the z-axis.

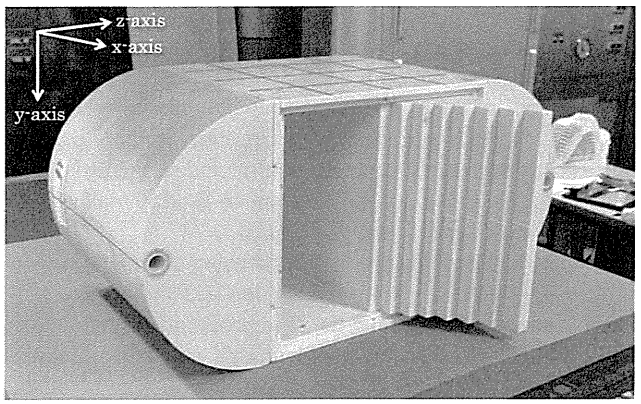

FIG. 3. Dose measurement phantom in the IMRT verification measurement. Two films were carefully placed at the fixed location in the box of the phantom and were sandwiched between 1 cm plates. After plan irradiation, four landmarks were pricked under a dark room to coregister the dose distribution from the film.

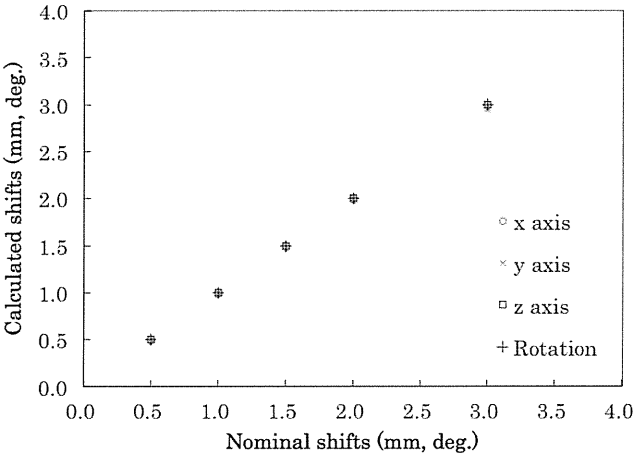

FIG. 4. Nominal and calculated xyz-shifts and rotation in the preliminary study. All xyz-shifts and rotations calculated using the OS method were in agreement with all nominal ones.

against the isocenter. Four different values for the shifts in x-, y-, z-axes (0.0, 0.5, 1.0, or 3.0 mm) and three different rotations (0.5°, 1.0°, or 3.0°) were used for 94 total combinations. Additionally, two combinations in shifts in all three axes and rotation (1.5 mm and 1.5°, 2.0 mm and 2.0°) were created. Finally, the OS method computed the xyz-shifts and rotation as the result of the comparison between the reference and the comparative images. To assess the validity of the OS method, the computed shifts and rotation were compared with nominal shifts and rotation.

II.C. Clinical study of the OS method

Thirteen clinical prostate IMRT plans that had been used to treat patients were chosen randomly. An Eclipse treatment planning system version 10.0 was used to create the treatment plans. The dose calculation grid size was set to be 2.5 mm. The plan measurement was performed using Kodak EDR2 film (Eastman Kodak Co., Rochester, NY) and an I'mRT Phantom. As shown in Fig. 3, the phantom was abdomen-shaped, where two films were placed parallel to the sagittal plane. The two films were located at isocenter and either 1 or 2 cm away from isocenter. Each of the plans was irradiated to the phantom containing the films. The films were developed and scanned by an Epson Expression 10000XL (Seiko Epson Co., Suwa, Nagano, Japan). The scanned film measurement and the calculated image were compared using Simple IMRT Analysis Version 2.0 including the OS method. The evaluations of DD and gamma index were done with and without the OS method. After the calculation of the OS method, the xyz-shifts and rotation computed by the OS method were evaluated. No normalization for dose distributions was applied.

III. RESULTS

III.A. Preliminary study of the OS method

Using the 94 and two additional combinations of xyz-shifts and rotation, the nominal shifts and rotation were compared with the shifts and rotation computed by the OS method. As shown in Fig. 4, all computed and nominal xyz-shifts and rotation were in agreement. For instance, the OS method showed the same values as the comparative image that was shifted by 0.5 mm in the x-, y-, and z-axes and 0.5° in rotation.

III.B. Clinical study of the OS method

As shown in Fig. 5, visual evaluation using 2D maps of DD and gamma index was performed for one of the planes. In terms of the DD evaluation, the regions in red and blue from the OS method result, where the pixel values were close to or beyond the tolerance value (3%), were smaller than those without the OS method. In particular, the regions beyond the tolerance value were located in high dose gradient regions. In

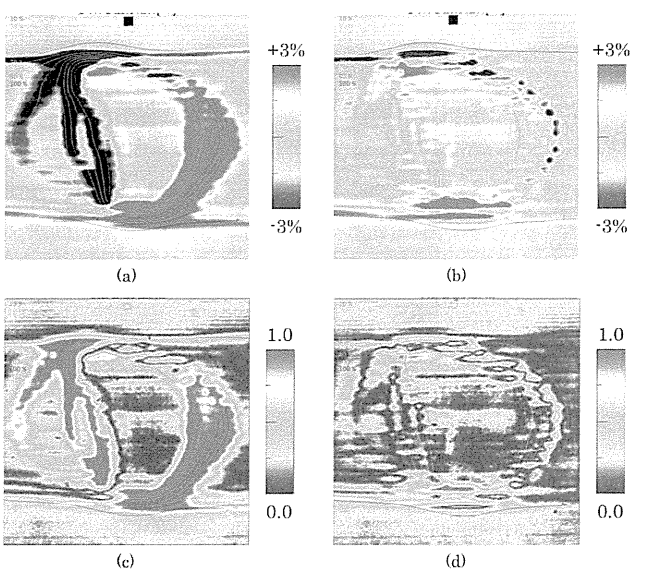

FIG. 5. 2D maps of DD without (a) and with (b) the OS method and of gamma index without (c) and with (d) the OS method.

TABLE I. Average values and pass ratios of DD and gamma index at each dose region and in the region from 30% to 100% without and with the OS method.

	DD				Gamma index			
	Value (ABS) [%]		Pass ratio [%]		Value		Pass ratio [%]	
Dose [%]	w/o the OS	w/ the OS	w/o the OS	w/ the OS	w/o the OS	w/ the OS	w/o the OS	w/ the OS
30–40	3.18	1.07	66.92	94.87	0.74	0.23	79.67	100
40–50	2.76	0.93	70.54	93.73	0.64	0.19	79.86	100
50–60	4.66	1.31	26.70	90.41	1.02	0.23	52.08	100
60–70	4.12	0.99	41.85	93.02	0.92	0.19	62.09	100
70–80	4.66	1.02	25.86	94.72	1.03	0.19	46.32	99.90
80–90	4.37	1.13	26.14	92.05	0.91	0.22	52.27	99.49
90–100	1.12	0.85	93.81	97.19	0.27	0.22	99.42	99.53
All	3.55	1.04	50.26	93.71	0.79	0.21	67.39	99.85

terms of the gamma index evaluation, the regions in red and blue with the OS method were also smaller than those without the OS method.

The pixel values of DD and gamma index in each dose region (30%–100%, 10% interval) were collected. Then, the average values and pass ratios of DD and gamma index were calculated. The pass ratio is the number of the pixels less than the tolerance values for DD and gamma index (DD: 3%, gamma index: 1.0) divided by the number of all pixels in each dose region. In terms of the average value of DD, all pixel values were absolute and were used to calculate the average value because positive and negative values of DD existed on the 2D map. If there were two pixel values on a 2D map of DD, which were −3% and +3%, the average value would be 0%. Similarly, the average values and the pass ratios of DD and gamma index for the dose region from 30% to 100% were calculated.

As shown in Table I, all of the values of DD below the 90% dose region without the OS exceeded the tolerance value in terms of average value. In contrast, all of the values with the OS method were within the tolerance value. In the comparison for the dose region from 30% to 100%, the value with the OS method had a 2.51% improvement using DD compared with the value without the OS method. In particular, the value with the OS method was 3.64% better than the value without the OS method at the 70%–80% dose region. With respect to the pass ratio of DD, all of the values with the OS method achieved over 90%. However, all of the values without the OS method except for the value in the region of 90%–100% were less than about 70%. The worst DD value was 26.14% at the region of 80%–90% without the OS method. In the region of 30%–100%, the values without and with the OS method were 43.45% and 93.71%, respectively, which means that the use of the OS method provided 50.26% improvement.

In terms of gamma index, all of the values with the OS method were below 0.23. Conversely, all of the values in the regions except for the region of 90%–100% were from 0.74 to 1.03 and were higher than those with the OS method. In addition, two of the regions were over the tolerance value. For the pass ratio of gamma index, all of the pass ratios with the OS method achieved over 99.5%. One region achieved over a 90% pass ratio without the OS method. The minimum in the pass ratios without the OS method was 46.32%.

Figure 6 shows the average values and pass ratios of DD and gamma index with one standard deviation at each dose region and in the region from 30% to 100% in the evaluations for the 26 planes. For DD and gamma index, all of the average values and standard deviations with the OS method were lower than those without the OS method. Still, all of the average values including the standard deviation with the OS were below 2.0% for DD and 0.5 for gamma index. However, two of the values of DD without the OS exceeded 3% and the values of DD without the OS method were larger than those with the OS method. Compared with the method without OS, the use of the OS method achieved 0.87% and 0.20% improvement for the average values of DD and gamma index, respectively. The pass ratios of DD and gamma index with the OS method were over 90% and 95%, respectively. Moreover, the pass ratio with the OS method showed 8.2% and 5.7% improvement against the values without the OS method. For the pass ratio of DD and gamma index, the use of the OS method showed better results in which there were higher pass ratios and smaller standard deviations in all regions. In particular, the amplitudes of the standard deviations with the OS method were small and similar in all regions compared with the method without OS.

Twenty-six sets of the values of xyz-shifts and rotation were acquired from the calculations for 26 planes using the OS method. Figure 7 shows that average values with one standard deviation at isocenter, off-axis, and a combination of both were found at each dose region and in the region from 30% to 100%. Except for the average value of the z-shift, all shift and rotational values were less than about 0.5 mm and 0.5°, respectively. The values of the z-shift at isocenter and off-axis were about 1 mm on average. The average value with one standard deviation at isocenter exceeded 2.0 mm. In particular, the standard deviation of the z-shift with the isocenter plane was around 1.5 mm. The z-shift amplitude was bigger than the amplitudes for x- and y-axes. Therefore, an additional experiment was performed in which a sheet of 0.04 mm-thick lead foil was inserted into the same location of the film at isocenter. An EPID image was then acquired and the location of the isocenter on the image was measured. Figure 8 shows that the geometric deviation between the actual and measured isocenter was 0.7 mm in the z-axis.

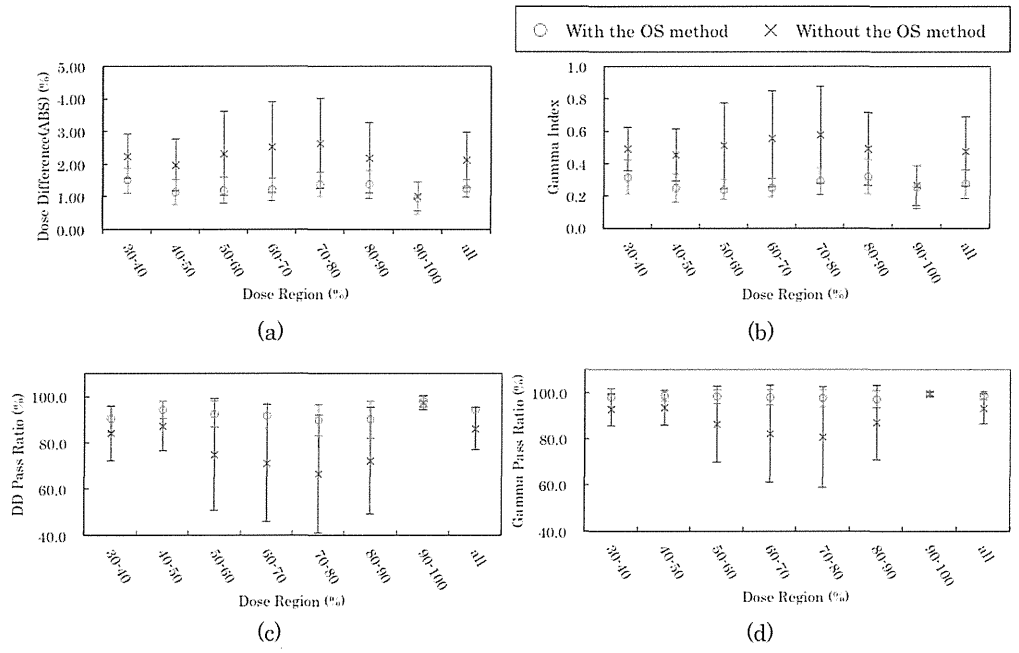

FIG. 6. DD (a), and gamma index (b) and pass ratio of DD (c) and gamma index (d) from the results of the retrospective analysis of the 26 planes.

IV. DISCUSSION

An end-to-end test for IMRT and VMAT is still common to verify a treatment plan before patient's treatment irradiation,[25,26] even though an independent computer program,[27] which verifies an IMRT plan without the measurement of the test, is commercially available to ease labor loads for the measurements for many patients. The end-to-end test provides information regarding comprehensive errors including a variety of errors from CT acquisition to dose delivery. In other words, it is not possible to extract specific errors from the end-to-end test. The OS method is able to extract the comprehensive geometric information of xyz-shifts and rotation from the test, but similarly cannot extract specific errors. This information includes geometric errors, such as setup errors for film, phantom, and 2D detector arrays; the error of isocenter laser alignment for CT simulator and linac; and the effects from inaccuracy for dose calculation algorithm, MLC motion calculation, and beam modeling.

In this study, the planar measurement data of dose distribution were acquired from EDR2 film. Currently, it is considered that film dosimetry gives us a relative dose distribution. However, some reports have shown that dose distributions acquired from EDR2 film could be close to the absolute dose distribution.[4,5,28] In particular, we should take care of the length of time between film exposure and processing to calibrate EDR2 film image to dose distribution properly. We created a protocol for EDR2 film dosimetry for our IMRT QA in accordance with the reports in the literature.[4,5,28] In this

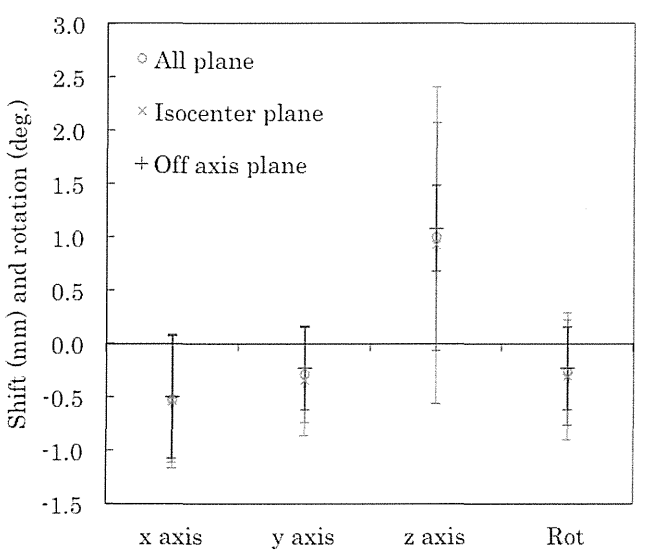

FIG. 7. xyz-shifts and rotation computed using the OS method in the retrospective analysis of the 26 planes.

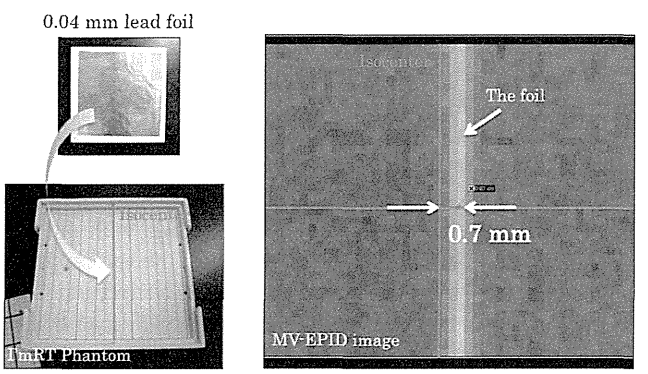

FIG. 8. Additional experiment where a sheet of 0.04 mm-thick lead foil was inserted along with the film at isocenter and an EPID-image was acquired. The EPID-image showed a 0.7 mm deviation between the isocenter and the location of the film at isocenter.

study, the dose distributions acquired should have been close to absolute dose distribution. Thus, inaccuracies derived from film dosimetry in this study were considered minimal. Additionally, not every measured dose distribution was normalized in this study. Even if a diode array dosimeter is used, the similar problem above would occur because we must calibrate the values acquired from the dosimeter to the values of absolute dose. The calibration would include some inaccuracies, and we may similarly normalize measured dose distributions acquired from the dosimeter. Therefore, the film measurements in this study did not affect the results from the OS method even though the OS method provided better results.

An advantage of film dosimetry compared with diode array dosimetry is that film dosimetry provides higher spatial resolution. A dose distribution acquired from film dosimetry represents a more spatially resolved dose distribution than that from a diode array dosimeter due to higher dose interpolation accuracy. With the OS method, the values of dose in the dose distribution reconstructed on x-, y-, z-axes were interpolated using B-spline. Therefore, higher spatial resolution of dose distribution is essential for the OS method and film dosimetry would make the OS method more accurate.

Using the OS method, the geometric information of the xyz-shifts and rotation were computed from the results of 27 sagittal planes in this study. Moreover, average and one standard deviation of the shift in the z-axis were bigger than those in the x- and y- axes, and the standard deviation of the shift in the z-axis was more than 1.0 mm. The geometric setup accuracy for the phantom was considered to be within 1 mm. Even if there is no systematic geometric error, random geometric error would still affect accuracy and would equally affect accuracies on the xyz-axes. In the measurements of our IMRT QA, the phantom setups were carefully performed using the isocenter lasers that are checked daily and recalibrated monthly in accordance with the report from AAPM TG-142. Thus, systematic error was considered to be minimized. However, there may be some deviations of the phantom setup due to random error. The deviations would be represented as the standard deviation of the shift computed using the OS method. Based on this result, we performed an additional experiment and found that there was a systematic geometric deviation between the actual isocenter and the location of the film at isocenter. Hence, the film setup error would be dominant for the comprehensive geometric error because the value from the experiment almost matched the value computed by the OS method. The OS method can provide information regarding comprehensive errors but not specific ones, which would be lost if visual registration for the measured dose distribution from film or 2D detector arrays was performed to intentionally improve pass ratio after the location of the measured dose distribution was coregistered. If user-intentional registration is performed in the end-to-end test, the test cannot be defined as an end-to-end test; the meaning of the user-intentional registration is to ignore the geometric information throughout the test. The OS method is able to similarly coregister the dose distributions to get better results, however, along with quantitative geometric information. Therefore, the OS method is able to provide further information in addition to routine plan verification analysis using the general dose distribution comparison algorithms, such as DD, DTA, and gamma index.

In the clinical study of our prostate IMRT QA analysis, we found a systematic geometric error inside the phantom. In other words, all of the previous IMRT QA with the phantom included the systematic error. Because the OS method was developed and performed in the sagittal planes of clinical prostate IMRT, we realized the systematic error inside the phantom and will take steps to minimize the error.

Moreover, a systematic error affects the results in IMRT QA such as the gamma index passing rate. In general, tolerance values for gamma index, for example, 3-mm distance-to-agreement and 3% dose difference, are determined in each institute. If unexpected geometric errors occur during IMRT QA, the passing rate should be worse because the general dose distribution comparison algorithms cannot extract the geometric information. In other words, the geometric error is evaluated as a beam delivery error. Conversely, the OS method is able to quantitatively extract comprehensive geometric information and help find a specific geometric error from the results using the OS method. Visual registration for the dose measurement is nonquantitative and loses geometric information. In particular, there is a limitation of the visual registration to get a better result. This means that the visual registration is performed within the plane and not on a plane perpendicular to the measurement plane. The OS method handles both planes to achieve better results using the general dose distribution comparison algorithms along with quantitatively extracted geometric information. Therefore, the OS method will improve IMRT QA.

The comprehensive geometric error in the end-to-end test is both systematic and random. For example, the systematic error is derived from multiple phantom setup errors caused by continuous error of isocenter laser alignment, and also film location errors like the errors found in this study. Random error is caused by human setup deviations for phantom and film. Total random setup errors would be within 1 mm. Thus, if more than 1 mm is found as the geometric information from the OS method, some further geometric errors could occur. Additionally, as shown in this study, the results with the OS method are collected from several patient plans and the values on xyz-axes are compared with each other. The values should be similar, but like in this study, if a larger value is found, there could potentially be geometric errors. Therefore, the OS method is recommended to collect the geometric information and will improve IMRT QA.

In the common final analysis of the end-to-end test for IMRT and VMAT, a planar measured dose distribution is compared with a planar calculated dose distribution. In the comparison using 2D dose distributions, dose profiles perpendicular to the evaluation plane could affect the result. However, the effect perpendicular to the plane would be regarded as the effect on the plane when we use the general dose distribution comparison algorithms. There are some investigations for a special comparison algorithm of the 3D gamma index method.[20–24] However, the algorithm would regard geometric error, such as setup errors for film, phantom, and

isocenter laser alignment error, as errors of beam delivery, which means that the algorithm would not be able to extract geometric information of shifts and rotation. On the other hand, the OS method reconstructs a planar dose distribution from the volume dose distribution. Thus, the OS method could be regarded as the method to take 3D doses into consideration. In addition, the method could allow a comparison between measured and calculated planar dose distributions using all of the general dose distribution comparison algorithms that were represented in the guidelines.[25,26]

In terms of accuracy of the reconstructed dose distribution on the z-axis as well as xy-axes in the OS method, dose calculation grid size should be minimized. Then, values of dose interpolated by B-spline in the reconstruction process of the OS method are more accurate when a dose calculation volume data with the smaller grid size is used. However, Chung *et al.*[29] showed that a dose calculation grid size < 3 mm would be clinically sufficient to interpolate the values of dose in terms of the accuracy of dose calculation for head and neck IMRT dose distributions. A similar phenomenon is produced in the reconstruction of dose distribution in the OS method. The effect of grid size is small to ensure accuracy of the reconstructed dose distribution. Also, prostate IMRT plans were used to evaluate the effectiveness of the OS method in this study, and dose calculation grid size may have a lesser effect on prostate IMRT plans than on head and neck IMRT plans due to high dose gradient regions. Therefore, the grid size used in this study was sufficient for the OS method.

Additionally, a relatively small dose calculation grid size prolonged the time of dose calculation related to work efficiency. As time is clinically essential, grid size should be determined to balance accuracy of the OS method and work efficiency.

V. CONCLUSION

The OS method was developed to quantitatively extract geometric information related to beam targeting from an end-to-end test for IMRT and VMAT with a better evaluation result by using volumetric calculation data from a treatment planning system and planar measurement data from film and 2D detector arrays. In the end-to-end test, visual registration for the dose measurement from film and 2D detector arrays to get better evaluation results loses the geometric information throughout the test. However, the OS method achieves a better evaluation result along with geometric information of xyz-shifts and rotation.

In this study, the measurements of prostate IMRT plans were retrospectively analyzed with and without the OS method. Based on volumetric dose distribution compared with planer dose distribution, a shift in the z-axis was notified and a systematic error of film setup was found. Thus, when we statistically analyze multiple measurements for IMRT and VMAT plans using the OS method, we can get effective geometric information and the quality of the test will be improved. However, all methods, including the OS method, have a limitation that needs to be considered: they cannot indicate and measure amplitudes for specific errors.

ACKNOWLEDGMENTS

The authors wish to thank Yasushi Ito, Fumiyasu Matsubayashi, Masatoshi Hashimoto, Takeo Hashimoto, Yuko Ohtomo, Ryuzo Uehara, Tatsuya Kamima, and Tomoharu Sato at the Cancer Institute Hospital of the Japanese Foundation of Cancer Research.

[a]Author to whom correspondence should be addressed. Electronic mail: Hidenobu.Tachibana@UTSouthwestern.edu; Telephone: +1(214)633-1744.

[1]D. A. Low, W. B. Harms, S. Mutic, and J. A. Purdy, "A technique for the quantitative evaluation of dose distributions," Med. Phys. **25**, 656–661 (1998).

[2]N. Agazaryan, T. D. Solberg, and J. J. DeMarco, "Patient specific quality assurance for the delivery of intensity modulated radiotherapy," J. Appl. Clin. Med. Phys. **4**, 40–50 (2003).

[3]D. A. Low, J. M. Moran, J. F. Dempsey, L. Dong, and M. Oldham, "Dosimetry tools and techniques for IMRT," Med. Phys. **38**, 1313–1338 (2011).

[4]N. L. Childress, M. Salehpour, L. Dong, C. Bloch, R. A. White, and I. I. Rosen, "Dosimetric accuracy of Kodak EDR2 film for IMRT verification," Med. Phys. **32**, 539–548 (2005).

[5]C. Shi, N. Papanikolaou, Y. Yan, X. Weng, and H. Jiang, "Analysis of sources of uncertainty for EDR2 film-based IMRT quality assurance," J. Appl. Clin. Med. Phys. **7**, 1–8 (2006).

[6]C. Andres, A. del Castillo, R. Tortosa, D. Alonso, and R. Barquero, "A comprehensive study of the Gafchromic EBT2 radiochromic film: A comparison with EBT," Med. Phys. **37**, 6271–6278 (2010).

[7]C. L. Ong, W. F. Verbakel, J. P. Cuijpers, B. J. Slotman, F. J. Lagerwaard, and S. Senan, "Stereotactic radiotherapy for peripheral lung tumors: A comparison of volumetric modulated arc therapy with 3 other delivery techniques," Radiat. Oncol. **97**, 437–442 (2010).

[8]A. Sankar, K. M. Ayyangar, R. M. Nehru, P. G. Kurup, V. Murali, C. A. Enke, and J. Velmurugan, "Comparison of Kodak EDR2 and GAFCHROMIC EBT film for intensity-modulated radiation therapy dose distribution verification," Med. Dosim. **31**, 273–282 (2006).

[9]S. G. Ju, Y. Han, O. Kum, K. H. Cheong, E. H. Shin, J. S. Shin, J. S. Kim, and Y. C. Ahn, "Comparison of film dosimetry techniques used for quality assurance of intensity modulated radiation therapy," Med. Phys. **37**, 2925–2933 (2010).

[10]E. Spezi, A. L. Angelini, F. Romani, and A. Ferri, "Characterization of a 2D ion chamber array for the verification of radiotherapy treatments," Phys. Med. Biol. **50**, 3361–3373 (2005).

[11]V. Chandraraj, S. Stathakis, R. Manickam, C. Esquivel, S. S. Supe, and N. Papanikolaou, "Comparison of four commercial devices for RapidArc and sliding window IMRT QA," J. Appl. Clin. Med. Phys. **12**, 338–349 (2011).

[12]V. Chandraraj, S. Stathakis, R. Manickam, C. Esquivel, S. S. Supe, and N. Papanikolaou, "Consistency and reproducibility of the VMAT plan delivery using three independent validation methods," J. Appl. Clin. Med. Phys. **12**, 129–140 (2011).

[13]B. Poppe, A. Blechschmidt, A. Djouguela, R. Kollhoff, A. Rubach, K. C. Willborn, and D. Harder, "Two-dimension ionization chamber arrays for IMRT plan verification," Med. Phys. **33**, 1005–1015 (2006).

[14]J. L Bedford, Y. K. Lee, P. Wai, C. P. South, and A. P. Warrington, "Evaluation of the Delta4 phantom for IMRT and VMAT verification," Med. Phys. Biol. **54**, N167–N176 (2009).

[15]M. Geurts, J. Gonzalez, and P. Serrano-Ojeda, "Longitudinal study using a diode phantom for helical tomotherapy IMRT QA," Med. Phys. **36**, 4977–4983 (2009).

[16]R. Sadagopan, J. A. Bencomo, R. L. Martin, G. Nilsson, T. Matzen, and P. A. Balter, "Characterization and clinical evaluation of a novel IMRT quality assurance system," J. Appl. Clin. Med. Phys. **10**, 104–119 (2009).

[17]V. Feygelman, K. Forster, D. Opp, and G. Nilsson, "Evaluation of a biplanar diode array dosimeter for quality assurance of step-and-shoot IMRT," J. Appl. Clin. Med. Phys. **10**, 64–78 (2009).

[18]Y. Watanabe and N. Gopishankar, "Three-dimensional dosimetry of TomoTherapy by MRI-based polymer gel technique," J. Appl. Clin. Med. Phys. **12**, 14–27 (2011).

[19]Y. Watanabe, T. Akimitsu, Y. Hirokawa, R. B. Mooij, and G. M. Perera, "Evaluation of dose delivery accuracy of Gamma Knife by polymer gel dosimetry," J. Appl. Clin. Med. Phys. **6**, 133–142 (2005).
[20]A. L. Petoukhova, J. van Egmond, M. G. C. Eenink, R. G. J. Wiggenraad, and J. P. C. van Santvoort, "The ArcCHECK diode array for dosimetric verification of HybridArc," Phys. Med. Biol. **56**, 5411–5428 (2011).
[21]E. Spezi and D. G. Lewis, "Gamma histograms for radiotherapy plan evaluation," Radiother. Oncol. **79**, 224–230 (2006).
[22]S. Gillisa, C. D. Wagtera, J. Bohsunge, B. Perrinc, P. Williamsc, and B. J. Mijnheerd, "An inter-centre quality assurance network for IMRT verification: Results of the ESTRO QUASIMODO project," Radiother. Oncol. **76**, 340–353 (2005).
[23]A. Bakai, M. Alber, and F. Nüsslin, "A revision of the γ-evaluation concept for the comparison of dose distributions," Phys. Med. Biol. **48**, 3543–3553 (2003).
[24]M. Wendling, L. J. Zijp, L. N. McDermott, E. J. Smit, J.-J. Sonke, B. J. Mijnheer, and M. van Herka, "A fast algorithm for gamma evaluation in 3D," Med. Phys. **34**, 1647–1654 (2007).
[25]G. A. Ezzell, J. M. Galvin, D. Low, J. R. Palta, I. Rosen, M. B. Sharpe, P. Xia, Y. Xiao, L. Xing, and C. X. Yu, "Guidance document on delivery, treatment planning, and clinical implementation of IMRT: Report of the IMRT subcommittee of the AAPM radiation therapy committee," Med. Phys. **30**, 2089–2115 (2003).
[26]G. A. Ezzell, J. W. Burmeister, N. Dogan, T. J. LoSasso, J. G. Mechalakos, D. Mihailidis, A. Molineu, J. R. Palta, C. R. Ramsey, B. J. Salter, J. Shi, P. Xia, N. J. Yue, and Y. Xiao, "IMRT commissioning: Multiple institution planning and dosimetry comparisons, a report from AAPM Task Group 119," Med. Phys. **36**, 5359–5373 (2009).
[27]T. Pawlicki, S. Yoo, L. E. Court, S. K. McMillan, R. K. Rice, J. D. Russell, J. M. Pacyniak, M. K. Woo, P. S. Basran, J. Shoales, and A. L. Boyer, "Moving from IMRT QA measurements toward independent computer calculations using control charts," Radiother. Oncol. **89**, 330–337 (2008).
[28]N. L. Childress and I. I. Rosen, "Effect of processing time delay on the dose response of Kodak EDR2 film," Med. Phys. **31**, 2284–2288 (2004).
[29]H. Chung, H. Jin, J. Palta, T. S. Suh, and S. Kim, "Dose variations with varying calculation grid size in head and neck IMRT," Phys. Med. Biol. **51**, 4841–4856 (2006).